Fabrication of widely tunable ridge waveguide DBR lasers for WDM-PON

Liangshun Han (韩良顺), Song Liang (梁 松)*, Can Zhang (张 灿),
Liqiang Yu (余力强), Lingjuan Zhao (赵玲娟), Hongliang Zhu (朱洪亮),
Baojun Wang (王宝军), Chen Ji (吉 晨), and Wei Wang (王 圩)

Key Laboratory of Semiconductor Materials Science, Institute of Semiconductors,
Chinese Academy of Science, Beijing 100083, China
*Corresponding author: liangsong@semi.ac.cn

We report the fabrication of widely tunable ridge waveguide distributed Bragg reflector (DBR) lasers with InGaAsP butt-joint as grating material. The shape of the butt–joint interface is found to have significant effect on the properties of the lasers. It is shown that irregular mode jumps during wavelength tuning can be avoided by a V-shaped butt–joint interface. From the fabricated device, 23 channels with 0.8 nm spacing and greater than 35 dB side mode suppression ratios are obtained. The different tuning characteristics of the ridge waveguide and the previously reported buried ridge stripe DBR lasers are discussed. Combined with the wide tuning range and the simple structure, the ridge waveguide DBR lasers are promising for use in wavelength division multiplexing passive optical networks (WDM-PONs).

OCIS codes: 230.1480, 140.3600, 230.7370, 230.0250.
doi: 10.3788/COL201412.091402.

Tunable lasers are key components of modern wavelength division multiplexing (WDM) optical communication system[1]. Tunable lasers help to reduce the inventory in both the construction and the operation of the WDM system. When single wavelength light sources such as distributed feedback (DFB) lasers are used, tens of different kinds of devices with different emission wavelengths have to be manufactured and inventoried, which increases related cost greatly. Compared with the tunable lasers with two sampled reflectors[2–5] and other tunable light sources[6,7], the two or three section distributed Bragg reflector (DBR) lasers have a more simple structure[8–11], leading to a lower cost in both the fabrication and calibration processes of the devices. This makes the DBR lasers more suitable for use in WDM-passive optical networks (PONs), which is a promising candidate for next generation access networks and needs a large number of low-cost light sources.

For WDM-PON applications, a wider wavelength tunable range of the DBR lasers is desired to realize colorless optical network units. It is known that with a fixed inject current in the DBR section, the range of wavelength tuning is proportional to the bandgap (in micrometers) of the DBR material[12,13]. By butt–joint bulk InGaAsP material with 1.43 μm bandgap (1.43Q) as DBR material, buried ridge stripe (BRS) DBR lasers with over 15 nm wavelength tuning range have been fabricated[14]. However, the presence of a large number of nonradiative recombination defects at the lateral buried stripe interface in the DBR section is unavoidable, which is shown to shorten the lifetime of the DBR lasers noticeably by causing wavelength drift with time[15]. A natural way to increase the lifetime of the butt-jointed tunable DBR lasers is the application of a ridge waveguide structure instead of a buried ridge one[15]. For the ridge waveguide structure, regrowth of the cladding layer and contact layer is carried out on a planar surface, thus avoiding the generation of nonradiative recombination defects in the DBR region of the devices.

In this letter, we report the first fabrication of ridge waveguide DBR lasers with 1.4Q InGaAsP butt–joint as DBR material. A 13.8 nm wavelength tuning range is obtained from the device by changing the inject current of the DBR section only. Accompanied by adjusting the temperature of the device, the range can be expended to 17.6 nm, covering 23 channels with 0.8 nm spacing. The different tuning characteristics of the ridge waveguide devices and the BRS devices are presented and discussed.

The DBR lasers were fabricated by a three-step metal organic chemical vapor deposition (MOCVD) process. In the first MOCVD run, multiple quantum wells (MQWs) were grown on an n-type InP substrate, which consisted of six 4 nm compressively strained InGaAsP wells ($+1.1 \times 10^{-2}$, $\lambda_{PL} = 1.59$ μm, PL stands for photoluminescence), seven 8 nm InGaAsP barrier layers (-3×10^{-3}, $\lambda_{PL} = 1.2$ μm), were sandwiched between two 80 nm InGaAsP separate confinement heterostructure (SCH) layers ($\lambda_{PL} = 1.2$ μm) lattice matched to InP.

Then, with the protection of SiO_2 films with 150 nm thickness, the In GaAsP SCH layers and the MQW layer in the DBR section were selectively removed by reaction ion etching (RIE) with the CH_4/H_2 gas mixture. The wafer was then treated by H_2SO_4: H_2O_2: $H_2O = 3:1:1$ solution for 50 s to remove the surface defects generated
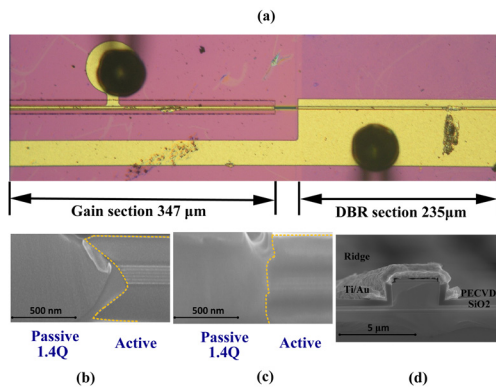
Fig. 1. (a) Optical microscope image of a fabricated two-section DBR laser, SEM image of a butt–joint interface treated by $H_2SO_4{:}H_2O_2{:}H_2O = 3{:}1{:}1$ solution for (b) 50 and (c) 10 s, and (d) cross-section SEM image of the device waveguide.

during the RIE process and form a side wall with a proper shape. With the SiO_2 films covering the gain sections, a 400 nm 1.4Q InGaAsP waveguide core layer lattice matched to InP was butt–jointed with the active layer of the gain sections in the second MOCVD growth. Because epimaterials do not nucleate on the SiO_2 films during MOCVD growth, no InGaAsP is deposited over the gain regions. Details of a typical butt–joint process can be found in Ref. [16]. A typical scanning electron microscope (SEM) image of the butt–joint interface is shown in Fig. 1(b). As can be seen, no defects such as voids can be seen, which ensures a high-efficiency light coupling between the active gain section and the DBR section. After a grating was formed in the 1.4Q layer of the DBR section by holographic lithography and dry etching, a p-type InP cladding layer and a p$^+$-type InGaAs contact layer were grown in the final MOCVD growth run. A 3 μm wide ridge waveguide was fabricated by wet etching, which is terminated above the upper SCH layer in the gain section and the 1.4Q layer in the

DBR section. Figure 1(d) shows an SEM image of the cross-section of the ridge waveguide. An optical microscope image of a finished device is shown in Fig. 1(a). No phase section is adopted in the device and the separation between the two sections is 50 μm, in which He$^+$ is implanted to increase the electrical isolation. The devices were mounted on Cu heat sink for measurements. Both facets of the devices were left uncoated.

Figure 2(a) shows the laser emission wavelength and the corresponding side mode suppression ratio (SMSR) as a function of the inject current of the DBR section of a DBR laser measured at 40 °C. As can be seen, the emission is around 1.54 μm and the wavelength can be tuned for 13.8 nm for a Bragg current of 160 mA. During the tuning process, the decrease in the output power of the laser is about 1.6 dB. Except in the narrow regions where mode jump happens, the SMSR is higher than 35 dB for the whole tuning range. By setting the lengths of the DBR section and gain section as 235 and 347 μm, respectively, emission modes regularly spaced by 0.8 nm are obtained.

The tuning range of our device is noticeably larger than the DBR lasers fabricated by other than butt–joint techniques[8,9], whose tuning range is limited to about 10 nm. It is, however, apparently smaller than the BRS DBR lasers fabricated by butt–joint technique[14,15]. With a similar thickness of 1.43Q InGaAsP as DBR material, an over 15 nm tuning range is obtained for only 70 mA Bragg current[14]. In the reported BRS DBR lasers, the DBR waveguide is only 1.5 μm wide and H$^+$ implantation is used to define a narrow current flow channel around the DBR waveguide, which leads to a larger carrier density variation and thus a larger wavelength change for a given current difference. In our ridge waveguide DBR lasers, however, the current diffuses in the DBR material freely, leading to a lower tuning efficiency. As shown in Fig. 2(a), a 160 mA Bragg current is needed for the 13.8 nm tuning range. Further increase in the DBR inject current would not increase the tun-
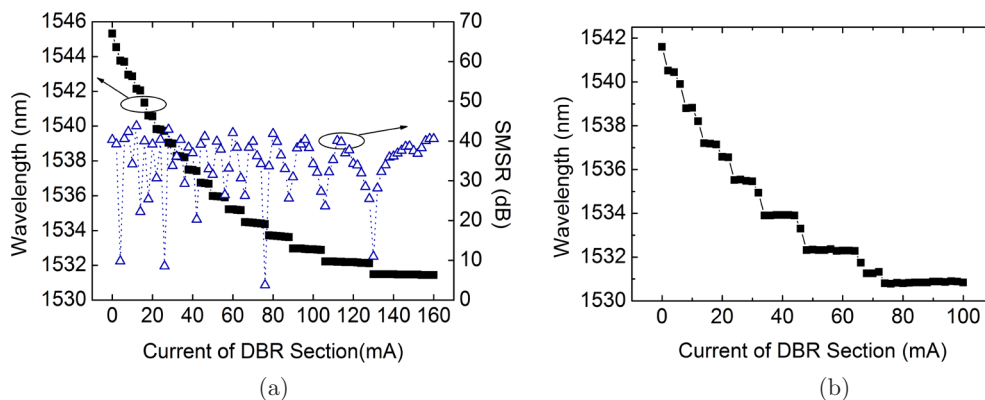

Fig. 2. (a) Emission wavelength and SMSR as a function of DBR current of a device with V-shaped butt–joint interface and (b) emission wavelength as a function of DBR current of a DBR laser with vertical butt–joint interface. The measurements were conducted at 40 °C with gain current is fixed at 75 mA
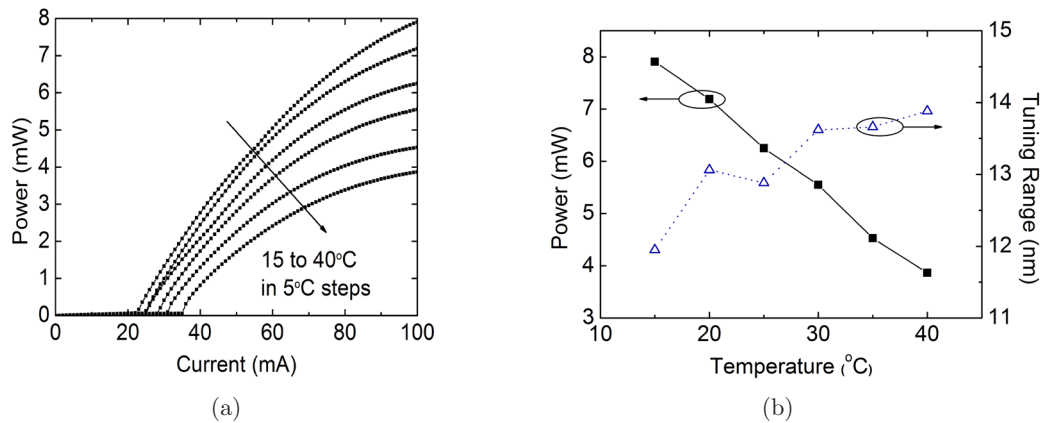
(a)　　　　　　　　　　　　　　　　(b)

Fig. 3. (a) Light output power as a function of gain current at different temperatures when no current is injected in the DBR section and (b) output power and tuning range of the DBR laser as a function of temperature with 100 mA gain current. For tuning range measurement, the DBR section current is varied from 0 to 160 mA.

ing range because of the self-heating effect which counteracts the effect of inject current on refractive index. To expand the wavelength tuning range further, a narrower ridge waveguide can be adopted and InGaAsP with narrower bandgap (longer emission wavelength) can be used as DBR material[12,13].

When InGaAsP bulk material is butt–jointed as DBR material, the shape of the butt–joint interface is found to be able to effect the properties of the fabricated DBR lasers greatly. Figure 1(c) shows a SEM picture of a butt–joint interface, which is treated by the H_2SO_4:H_2O_2:H_2O=3:1:1 solution for 10 s before the butt–joint regrowth. As can be seen, the interface is nearly vertical to the substrate. The laser wavelength as a function of the DBR section current of a fabricated DBR laser is shown in Fig. 2(b). There are frequent irregular mode jumps which are larger than the expected 0.8 nm as the DBR current is increased. The irregular mode jumps can be attributed to the reflection of light into the cavity at the butt–joint interface, which may alter the otherwise evenly spaced FP modes of the lasers[17]. By increasing the treating time of the H_2SO_4:H_2O_2:H_2O=3:1:1 solution to 50 s, a V-shaped butt–joint interface can be obtained as shown in Fig. 1(b). At the interface with this shape, the reflection of light back into the laser cavity is reduced, leading to the desired evenly spaced mode jump as shown in Fig. 2(a).

With no DBR current injection, the light output power as a function of gain current of the DBR laser at different temperatures are shown in Fig. 3(a). The light power and tuning range of the DBR laser as a function of temperature with 100 mA gain current is summarized in Fig. 3(b). As can be seen, the output power decreases from 7.9 to 3.9 mW and the tuning range increases from 11.9 to 13.8 nm when the temperature is increased from 15 to 40 °C. What is more, for fixed gain and Bragg currents, the emission wavelengths of the laser are redshifted for about 3.2 nm by the thermal effect. This indicates that the tuning range of the

DBR laser can be expanded effectively by simply varying the temperature. As shown in Fig. 4, 23 × 0.8 nm spaced channels are obtained, with SMSR > 35 dB. The lifetime properties of our DBR lasers have not been studied yet. However, because the generation of nonradiative recombination defects in the DBR section can be avoided, ridge waveguide DBR lasers are expected to have a longer lifetime than the DBR lasers with buried waveguide structures[15].

In conclusion, we fabricate widely tunable ridge waveguide two section DBR lasers with butt–jointed 1.4Q InGaAsP bulk material as DBR material. By optimizing the fabrication process, we obtain a V-shaped butt–joint interface, which is shown to eliminate the irregular mode jumps during wavelength tuning. From the device, 23 channels with 0.8 nm spacing and larger than 35 dB SMSR are obtained. The simple structure and the wide tuning range make the ridge waveguide DBR lasers promising for use in WDM-PON.
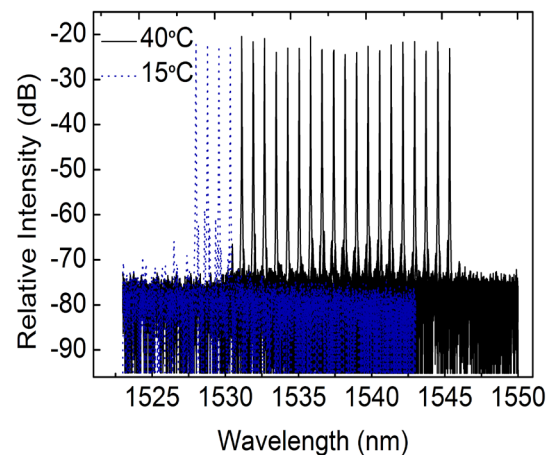

Fig. 4. Lasing spectra of the DBR laser with 0.8 nm spacing under 15 and 40 °C.

References

1. L. A. Coldren, IEEE J. Sel. Top. Quant. Electron. **6,** 988 (2000).
2. V. Jayaraman, Z.-M. Chuang, and L. A. Coldren, IEEE J. Quant. Electron. **29,** 1824 (1993).
3. B. Mason, G. A. Fish, S. P. DenBaars, and L. A. Coldren, IEEE Photon. Technol. Lett. **10,** 1211 (1998).
4. L. Yu, D. Lu, B. Pan, and L. Zhao, IEEE Photon. Technol. Lett. **26,** 722 (2014).
5. J. W. Raring, L. A. Johansson, E. J. Skogen, M. N. Sysak, H. N. Poulsen, Steven P. DenBaars, and L. A. Coldren, J. Lightwave Technol. **25,** 239 (2007).
6. C. Zhang, S. Liang, L. Ma, L. Han, and H. Zhu, Chin. Opt. Lett. **11,** 041401 (2013).
7. P. Yang, S. Xiao, H. Feng, M. Bi, J. Shi, and Z. Zhou, Chin. Opt. Lett. **11,** 040602 (2013).
8. S. Murata, I. Mito, and K. Kobayashi, Electron. Lett. **24,** 210 (1988).
9. T. L. Koch, U. Koren, and B. I. Miller, Appl. Phys. Lett. **53,** 1036 (1988).
10. D. J. Robbins, J. P. Duck, N. D. Whitbread, A. J. Ward, B. Rousseau, and F. Lelarge, IEEE Photon. Technol. Lett. **20,** 147 (2008).
11. H. Klein, C. Wagner, W. Brinker, F. Soares, D. de Felipe, Z. Zhang, C. Zawadzki, N. Keil, and M. Moehrle, in *Proceedings of 2012 International Conference on Indium Phosphide and Related Materials* 20 (2012).
12. J.-P. Weber, IEEE J. Quant. Electron. **30,** 1801 (1994).
13. G. Kyritsis and N. Zakhleniuk. IEEE J. Sel. Top. Quant. Electron. **19,** 1 (2013).
14. F. Delorme, G. Alibert, P. Boulet, S. Grosmaire, S. Slempkes, and A. Ougazzaden, IEEE J. Sel. Top. Quant. Electron. **3,** 607 (1997).
15. F. Delorme, G. Terol, H. de Bailliencourt, S. Grosmaire, and P. Devoldere, IEEE J. Sel. Top. Quant. Electron. **5,** 480 (1999).
16. Y. Barbarin, E. A. J. M. Bente, T. de Vries, J. H. den Besten, P. J. van Veldhoven, M. J. H. Sander-Jochem, E. Smalbrugge, F. W. M. van Otten, E. J. Geluk, M. J. R. Heck, X. J. M. Leijtens, J. G. M. van der Tol, F. Karouta, and Y. S. Oei, in *Proceedings of the 10th Annual Symposium IEEE/LEOS Benelux* 89 (2005).
17. H. K. Choi, K.-L. Chen, and S. Wang, IEEE J. Quant. Electron. **20,** 385 (1984).